PROCEEDINGS, 50th Workshop on Geothermal Reservoir Engineering
Stanford University, Stanford, California, February 10-12, 2025
SGP-TR-229

Optimizing Mass Flow Rate in Enhanced and Advanced Geothermal Systems using Scaling Parameters

P. V. (Suri) Suryanarayana and Sharat Chandrasekhar

Blade Energy Partners, 2600 Network Blvd, Ste 550, Frisco TX 75034

pvsury@blade-energy.com

Keywords: Enhanced Geothermal Systems, Performance Optimization

ABSTRACT

In a previous work (Chandrasekhar, et al., GRC 2024 Proceedings), we presented scaling curves applicable to all enhanced geothermal systems (EGS) and advanced geothermal systems (AGS). We show that a nondimensional parameter, Γ (analogous to the Number of Transfer Units in heat exchanger analysis) scales both thermal performance and decline in EGS and AGS systems. In that work, both thermal performance and decline are evaluated in terms of a nondimensional temperature, θ. We showed that engineered heat extraction systems in both EGS and AGS decline with time (because Γ decreases with time), reaching a pseudo-steady state in one to several years (in terms of θ). The pseudo-steady state θ can sometimes be much lower than θ at initial production, depending upon how the system is operated. This poses problems in operational management of mass rates and exit pressure. The field development plan will have to be engineered such that nameplate power is delivered. However, this cannot be achieved using the θ vs Γ formulation, as it does not give insight into the behavior of enthalpy with time.

Given the thermal performance and decline of EGS/AGS systems, it is reasonable to expect that there exists a mass rate (or more generally, a mass rate schedule) that achieves two goals: maximize thermal performance; and minimize decline over a 20 to 30-year life. In this follow-up work, we consider the problem of optimization of mass flow rates, and their operational management to maximize enthalpy generation while minimizing decline.

We solve the nondimensionalized governing equations using a semi-analytic approach with appropriate initial condition and boundary conditions. The transient response (temperature gradient in the resource as a function of time) is captured using a time dependent "flux multiplier" which simplifies the solution. From this, a non-dimensional expression for enthalpy as a function of the ratio of Biot and Peclet numbers is derived. This is integrated over time to obtain cumulative enthalpy. The optimization problem is then posed as maximization of cumulative enthalpy (over a service duration). Several case studies that are representative of different EGS/AGS concepts being currently considered are presented. It is shown that by appropriately managing the mass flow rate, it is possible to optimize enthalpy production over a specified service duration, even though thermal decline is inevitable and will erode thermal performance over time. It is also shown that by being less aggressive with rates and enthalpy production in early life, the decline can be managed.

The authors hope that this work, taken together with the previous work, provides EGS/AGS designers and engineers with an easily applied approach to optimize operations. This work does not replace more sophisticated multi-physics simulation models that will need to be customized to the specifics of a given location. However, it provides an approach for a first pass evaluation of different concepts and their operational management. Indeed it is believed that this is the first paper since Gringarten's seminal paper (Gringarten et al. (1975)) to systematically examine EGS and AGS systems, in a manner consistent with current operational feasibility.

1. INTRODUCTION

There is growing realization across the energy industry that we are in the midst of an epochal energy transition, one which is expected to radically alter sources, transmission and storage of energy. Geothermal energy is increasingly being recognized as a critical part of this transition. Geothermal energy is attractive because it provides dispatchable baseload, unlike many other renewable energy sources that are an important part of the energy transition. Recent developments in Advanced Geothermal Systems (or AGS), and classical Enhanced Geothermal Systems (EGS) have made it possible to extract geothermal energy from hot, dry rock (with no hydrothermal source). Many variants of these systems have been proposed, all of which essentially connect two (or more) wells through an engineered heat exchanger in the resource. Recent advances include connecting multilaterals between injector and producer (Holmes, et al., 2021), thermal reach enhancement (Moncarz and Suryanarayana, 2022), closed loop geothermal (Beckers, et al., 2022), down-borehole exchange (all of which are increasingly referred to as Advanced Geothermal Systems, or AGS), and the classical Enhanced Geothermal Systems (EGS) that connect two (or more) wells through some form of fracturing or stimulation. From its first demonstration in Fenton Hill (Brown, et al., 2012), EGS has come closer to commercial reality with the recent successes of Fervo (Norbeck et al, 2023) and Utah FORGE (Allis and Moore, 2019). Both these demonstration projects were at temperatures around 200°C. More recently, the potential of using EGS in superhot rock (with resource temperatures greater than 375°C) has emerged as a commercially viable and scalable technique for the production of geothermal energy (US Department of Energy, 2024). Moncarz and Suryanarayana (2022) describe a novel AGS technique for exploiting superhot rock. In 2024, the US DOE awarded a grant to Mazama Energy to demonstrate superhot rock, and recently (2025) ARPA-E announced a new funding opportunity in superhot rock. These recent events demonstrate that geothermal energy from superhot rock has become a national priority.

All EGS and AGS methods involve the circulation of a working fluid through an engineered "heat exchanger" in the resource to extract heat from it, which is then converted into electric power using an appropriate power cycle. The most commonly used working fluid is water. As heat is extracted from the resource, temperature, and hence produced power decline, requiring proper design and operational management of the AGS or EGS development to maintain capacity. In a recent paper (Chandrasekhar, et al., 2024), the authors show that all AGS and EGS concepts scale according to a non-dimensional scaling parameter Γ (analogous to the Number of Transfer Units, or NTU, commonly used in traditional heat exchanger analysis). The non-dimensional parameter Γ is a function of three nondimensional groupings that have physical significance in heat extraction from a geothermal resource: a) the ratio of the thermal contact area to flow area; b) the ratio of the thermal conductivity of the formation material to that of the working fluid; and c) the ratio of the Biot to Peclet numbers. The authors present a universal scaling curve, using which they demonstrate the performance of different AGS and EGS concepts in terms of a non-dimensional temperature, θ. They also present the thermal decline of the resource with time in terms of a non-dimensional thermal penetration depth, and the Fourier number. The authors conclude that this work provides a useful, generalized basis for quickly evaluating different thermal recovery concepts, and examining the impact of different modifications or improvements to heat recovery and recovery efficiency.

While the Chandrasekhar et al. (2024) work provides valuable insight into thermal performance of AGS and EGS methods, it does not provide insight into how the system can be operated to optimize power, Managing the exit temperature is not the same as maintaining or maximizing the produced enthalpy or electric power. This will require recasting the scaling analysis in terms of a non-dimensional mass rate. Exit temperature is still important, as it impacts the efficiency of conversion from heat to electricity.

In this work, we consider the problem of optimization of mass flow rates, and their operational management to maximize enthalpy generation while minimizing thermal decline. The scaling approach used in the previous work is extended to determine an optimal range of Γ that maximizes total energy produced over a period of time (usually 20 – 30 years). As before, we solve the nondimensionalized governing equations using a semi-analytic approach with appropriate initial condition and boundary conditions. The transient response (temperature gradient in the resource as a function of time) is captured using a time dependent "flux multiplier" which simplifies the solution. From this, a non-dimensional expression for enthalpy as a function of the ratio of Biot and Peclet numbers is derived. This is integrated over time to obtain cumulative enthalpy. The optimization problem is then posed as maximization of cumulative enthalpy (over a service duration). Several case studies that are representative of different EGS/AGS concepts being currently considered are presented. It is shown that by appropriately managing the mass flow rate (which is arguably the only remaining control variable once a system is installed), it is possible to optimize enthalpy and power production over a specified service duration, even though thermal decline is inevitable and will erode thermal performance over time.

In what follows, the mathematical model and solution approach are described first. Both fracture connectivity and drilled lateral connectivity are included in the formulation. A compact expression for the nondimensional parameter Γ is derived in terms of a modified Peclet number (which is a proxy for the mass flow rate, a control variable). An expression for nondimensional produced power (as a function of the nondimensional parameter Γ and time) is then derived in terms of the governing non-dimensional parameters. It is shown that the parasitic (frictional) power loss from flow through the resource is negligible. The injector and production riser will of course add parasitic losses, but these are common to both EGS and AGS systems, and can be treated as an additive constant. An expression for nondimensional power is then developed in terms of Γ. Efficiency of heat conversion is assumed to be a fraction of the Carnot efficiency, modeled as a cubic polynomial in the exit temperature. Optimum Γ is then obtained by setting the derivative of nondimensional power (with respect to Γ) to zero (noting that the additive constant vanishes upon differentiation). The decline in performance is also considered, by relating the modified Peclet number (and hence Γ) to the Fourier number. It is shown that the optimum Γ as a function of time falls within a narrow range. By managing operations such that Γ is at or near its optimum value as a function of time, the power performance of an EGS or AGS system can be maximized. Two examples are presented to illustrate the method.

2. MATHEMATICAL MODEL

2.1 Geometry of the Problem

Without loss of generality, an engineered "heat exchanger" created in a geothermal resource can be represented by two wellbores in the resource connected by one to several lateral conduits. The conduits can represent a single closed loop (as in a Closed Loop Geothermal System, or CLGS), a connected multilateral system (where the well pair is connected by drilled cylindrical lateral conduits), or a pair of wells connected by fractures (which can be represented as planar conduits connecting the well pair). Figure 1 (left panel) shows a notional closed loop geothermal well with two vertical wellbores connected by a multilateral system consisting of several widely spaced lateral conduits of specified length and diameter, as indicated in the figure. An example of this concept is presented by Holmes et al. (2021).

The network can also consist of several fractures connecting the two vertical wells, as shown in the right panel of Figure 1. In this case, the fractures are assumed to be notionally planar with specified aperture or width (typically 3—5 mm), length, and breadth of the planar fracture. Length and breadth are usually of the order of 100 m. Although the figure shows two vertical wells connected by planar fractures, the orientation of the wellbores and fractures can be arbitrary, as long as the fractures can be idealized as planar, rectangular conduits.

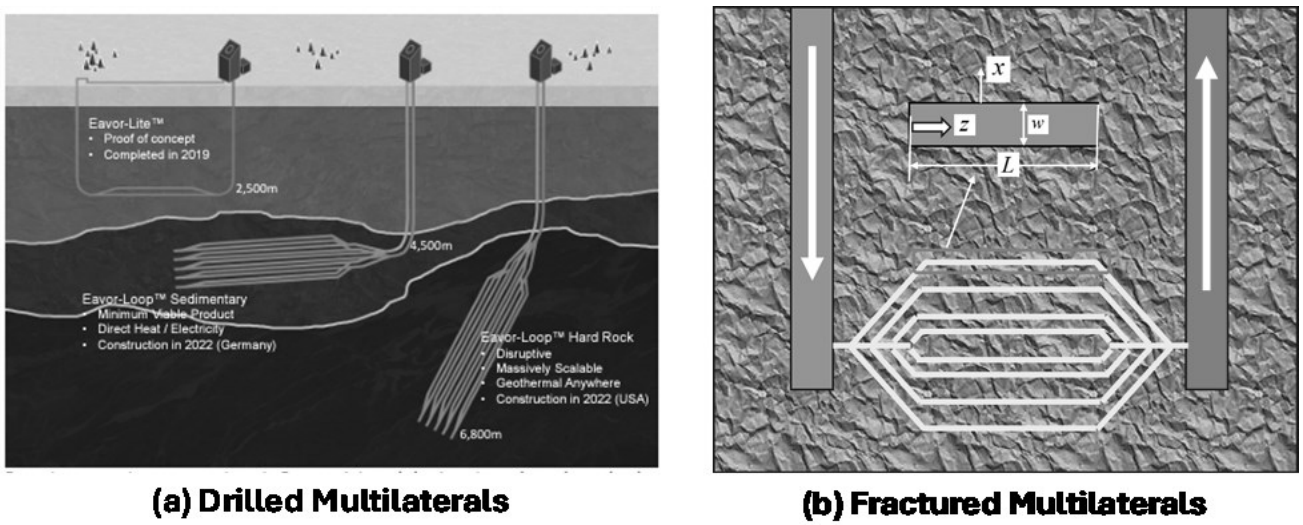

Figure 1: Multilateral Configurations connecting two Vertical Wellbores.

The key geometrical parameters of the two types of connectivity are shown in Figure 2. The drilled laterals have a specified diameter D. Since the breadth of the fracture is generally several orders of magnitude larger than the aperture width, the hydraulic diameter of the planar fracture can be approximated as $D_h \approx 2w$.

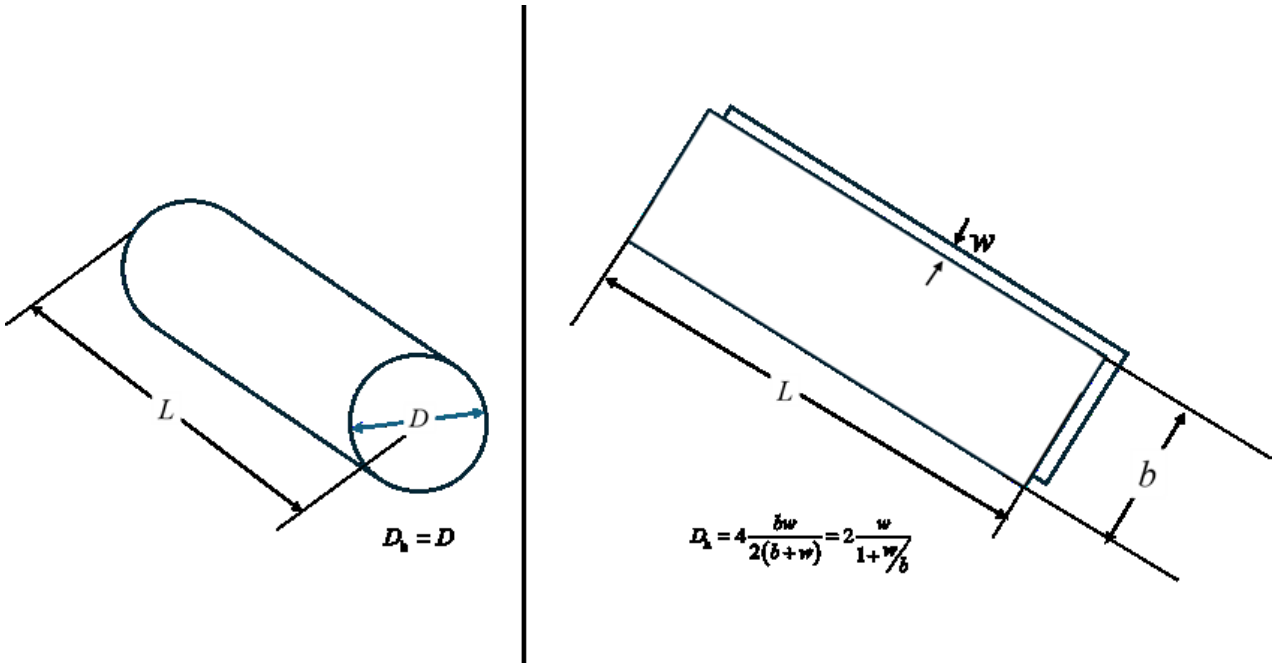

Figure 2: Geometry of a single Cylindrical (Drilled, Left) and Planar (Fractured, right) Conduit.

2.2 Governing Equations

Consider hydrodynamically fully developed flow in each horizontal conduit segment in Figure 1, under which the following assumptions are valid:

1. The resource is homogeneous, with constant thermophysical properties,
2. The flow is one-dimensional, with no thermophysical property variations or phase change in transverse directions,
3. The diameter of each conduit, or the width (aperture) of each fracture, is constant,

4. The sensible heat approach allows the enthalpy gradient to be represented by temperature and pressure gradients,
5. Transients are relegated to the formation and hence only to the conduit-formation interface flux, and
6. Separation between laterals is large enough that there is no thermal interference between individual conduits or fractures.

With the above assumptions, the quasi-steady (or pseudo-steady) non-conservative form of the transport equations of mass, momentum (Navier-Stokes), and energy in a *single lateral conduit* reduce to

$$\frac{\mathrm{d}\dot{m}}{\mathrm{d}t} = 0 \Rightarrow \dot{m} = \frac{\dot{m}}{\rho A_\mathrm{f}} \tag{1}$$

$$\frac{\mathrm{d}P}{\mathrm{d}z} = -\frac{1}{2} f \rho \frac{V^2}{D_\mathrm{h}} \tag{2}$$

and

$$\rho c_\mathrm{p} V \frac{\mathrm{d}T}{\mathrm{d}z} - \rho c_\mathrm{p} c_\mathrm{JT} V \frac{\mathrm{d}P}{\mathrm{d}z} = 2\pi^n \frac{U(t)}{A_\mathrm{f}} \left(T_\infty - T\right) \tag{3}$$

subject to the boundary condition

$$T\left(z=0\right) = T_0 \tag{4}$$

All entities in Eqs. (1)--(4) are defined in the nomenclature. The index n is a convenience to represent both geometries. It is equal to 1 for cylindrical drilled laterals and equal to 0 for planar fractures. In the latter context the factor 2 accounts for heat transfer across both surfaces of the fracture in contact with the formation. The Overall *Conductance* $U\left(t\right)$ is evaluated at some designated time instant t and takes the thermal decline of the flux at the conduit/formation interface into account, following the approach of Ramey (1961). The expressions for the conductance are provided in Appendix A for both cylindrical and planar geometries.

2.2 Streamwise Temperature Profile

If we define a dimensionless length and a dimensionless temperature as

$$\xi = \frac{z}{L} \tag{5}$$

and

$$\theta = \frac{T - T_\mathrm{in}}{T_\infty - T_\mathrm{in}} \tag{6}$$

then substitution of Eq. (2) into Eq. (3) leads to the dimensionless energy equation together with its boundary condition

$$\begin{aligned} &\frac{\mathrm{d}\theta}{\mathrm{d}\xi} = \Lambda + \Gamma\left(1-\theta\right) \\ &\theta\left(0\right) = 0 \end{aligned} \tag{7}$$

where the Frictional Heating Term is

$$\Lambda = \frac{1}{2} f \frac{L}{D_\mathrm{h}} \frac{V^2}{c_\mathrm{p} \Delta T} \tag{8}$$

and the parameter Γ which readers familiar with heat exchanger analysis will recognize as analogous to the Number of Transfer Units (NTU) is given by

$$\Gamma = 2\pi^n \frac{U(t) L}{\dot{m}_\mathrm{r}} \tag{9}$$

Eq. (7) has the solution

$$\theta = \left(1 + \frac{\Lambda}{\Gamma}\right)\left(1 - e^{-\Gamma\xi}\right) \tag{10}$$

The parameter Γ can also be expressed in terms of Biot and Peclet numbers as

$$\Gamma = 2\pi^n \frac{U(\bar{t})L}{\dot{r}} = 2\pi^n \underbrace{\frac{U(t)}{\dot{r}}}_{\mathrm{Bi}} \underbrace{\left(\frac{k_\infty L}{\dot{r}}\right)}_{1/\mathrm{Pe}_*} = 2\pi^n \frac{\mathrm{Bi}}{\mathrm{Pe}_*} \tag{11}$$

where the Biot Number and Modified Peclet Number are defined as

$$\mathrm{Bi} = \frac{U(t)}{k_\infty} \tag{12}$$

and

$$\mathrm{Pe}_* = \frac{\dot{r}}{k_\infty L} \tag{13}$$

While the definition of Pe_* in eq. (13) actually appears to be more consistent with that of Γ, substitution of $\dot{r}$ into Eq. (13) yields

$$\mathrm{Pe}_* = \frac{\dot{r}}{k_\infty L} = \frac{\rho c_\mathrm{p}}{k} \frac{k}{k_\infty} \frac{A_\mathrm{f}}{L} \tag{14}$$

For cylindrical and planar conduits respectively, substitution of the expressions for the flow area A_f gives the expressions

$$\mathrm{Pe}_* = \frac{\rho V c_\mathrm{p}}{k_\infty} \frac{k}{k_\infty} \frac{\pi d^2}{4L} = \underbrace{\pi\left(\frac{\rho V c_\mathrm{p} d}{k}\right)}_{\mathrm{Pe}_{\mathrm{Classical}}} \frac{k}{k} \frac{A_\mathrm{f}}{A_\mathrm{c}} \tag{15}$$

and

$$\mathrm{Pe}_* = \frac{\rho V c_\mathrm{p}}{k_\infty} \frac{k}{k_\infty} \frac{bw}{L} = \frac{b}{w}\underbrace{\left(\frac{\rho V c_\mathrm{p} w}{k}\right)}_{\mathrm{Pe}_{\mathrm{Classical}}} \frac{k}{k} \frac{A_\mathrm{f}}{A_\mathrm{c}} \tag{16}$$

where the terms in parenthesis are the classical definitions of the Peclet Number for flows in cylindrical and planar conduits. Consolidation and substitution into Eq. (11) yields the compact expression

$$\Gamma = 2\pi^n \frac{U(t)L}{\dot{r}} = 2\gamma_n \mathrm{Pe}^{-1}\mathrm{Bi}\left(\frac{k_\infty}{k}\right)\left(\frac{A_\mathrm{c}}{A_\mathrm{f}}\right) \tag{17}$$

in which the geometry factor and contact area are given by

$$\gamma_n = \left(\frac{w}{b}\right)^{1-n} \tag{18}$$

and

$$A_c = L\left[n\pi d + 2(1-n)b\right] \tag{19}$$

We see three important nondimensional groupings in the above equation: the ratio of the Biot number (Bi) to the Peclet number (Pe_*), the ratio of the formation conductivity to fluid conductivity, and the ratio of the thermal contact area (A_c) to the fluid flow area (A_f). Γ is directly proportional to the Biot number, the ratio of the areas, and the ratio of the conductivities. It is inversely proportional to the Peclet number (Pe_*). Since the higher the Γ, the more effective the thermal recovery (the higher the return temperatures), any strategy to improve thermal recovery has to necessarily increase Γ. This can be achieved by increasing the area ratio (for example, increasing the contact area while reducing flow area), the conductivity ratio (for example, enhancing effective formation thermal conductivity), or Bi, or by reducing Pe_* (for example, by increasing the number of connecting conduits or fractures). In a previous work (Suryanarayana, et al, 2023), the authors have noted the importance of reducing Pe_* to increase the nondimensional exit temperature. This work expands upon this notion, and shows that Γ is the fundamental governing nondimensional parameter for EGS and AGS, and that there exists an optimum range of Γ for a given system such that the *enthalpy and power* are maximized over a service duration. This approach to operational management is more effective than simply maximizing temperature, and is a key contribution of this work.

2.3 Parasitic Power Losses in Laterals

While the frictional pressure drop and associated parasitic power losses in the wellbore injector and riser are non-negligible at best and substantial at worst, the assumed equal division of the global mass flow rate amongst each of the lateral conduits results in a frictional pressure gradient across each conduit that is significantly smaller. The frictional pressure drop across a single lateral is given by

$$\Delta P = -\frac{1}{2} f \rho \frac{V^2}{D_\mathrm{h}} L \tag{20}$$

from which the parasitic power per lateral can be estimated as

$$\dot{W}_{\mathrm{Fric}} = -\dot{m}\frac{\Delta P}{\rho} = -\dot{m}\frac{1}{2} f \frac{V^2}{D_\mathrm{h}} L \tag{21}$$

With the exception of the two highlighted rows in Table 1 , it is seen that in practically all other cases of cylindrical laterals, the frictional losses are negligible. This is particularly true of planar conduits, as evidenced in the right panel of the table. As a consequence, the parameter Λ as defined in Eq. (8) is small enough to be neglected without any compromise in the temperature predictions. The computed values of the pressure drop, parasitic power, and the parameter Λ in Table 1 scale directly with conduit length , which for the purpose of the illustrative examples is 1 km. Accordingly the exit temperature in each of the laterals entering the riser ($\xi = 1$) can be approximated with high accuracy as

$$\theta(1) = 1 - e^{-\Gamma} \tag{22}$$

Table 1 Estimates of the Frictional Heating Parameter for Cylindrical (Left) and Planar (right) Conduits

Density (kg/m^3)	900
Specific Heat (J/kg-K)	4400
Temperature Difference (°C)	300
Conduit Length (m)	1000
Friction Factor	0.02
Width (Planar Conduits, m)	100

Drilled Cylindrical Conduits					
# Laterals	Mass Flow Rate (kg/s)	Conduit Diameter (in.)	ΔP (MPa)	Q. ΔP (MW)	Λ
5	50	2	5.3	0.3	4.48E-03
		4	0.2	0.0	1.40E-04
		6	0.0	0.0	1.84E-05
	75	2	**12.0**	**1.0**	**1.01E-02**
		4	0.4	0.0	3.15E-04
		6	0.0	0.0	4.15E-05
	100	2	**21.3**	**2.4**	**1.79E-02**
		4	0.7	0.1	5.60E-04
		6	0.1	0.0	7.38E-05
15	50	2	0.6	0.0	4.98E-04
		4	0.0	0.0	1.56E-05
		6	0.0	0.0	2.05E-06
	75	2	1.3	0.1	1.12E-03
		4	0.0	0.0	3.50E-05
		6	0.0	0.0	4.61E-06
	100	2	2.4	0.3	1.99E-03
		4	0.1	0.0	6.22E-05
		6	0.0	0.0	8.20E-06

Fractured Planar Conduits					
# Laterals	Mass Flow Rate (kg/s)	Conduit Width (mm)	ΔP (MPa)	Q. ΔP (MW)	Λ
25	50	2	6.94E-05	3.86E-06	5.85E-08
		4	8.68E-06	4.82E-07	7.31E-09
		6	2.57E-06	1.43E-07	2.16E-09
	75	2	**1.56E-04**	**1.30E-05**	**1.32E-07**
		4	1.95E-05	1.63E-06	1.64E-08
		6	5.79E-06	4.82E-07	4.87E-09
	100	2	**2.78E-04**	**3.09E-05**	**2.34E-07**
		4	3.47E-05	3.86E-06	2.92E-08
		6	1.03E-05	1.14E-06	8.66E-09
100	50	2	4.34E-06	2.41E-07	3.65E-09
		4	5.43E-07	3.01E-08	4.57E-10
		6	1.61E-07	8.93E-09	1.35E-10
	75	2	9.77E-06	8.14E-07	8.22E-09
		4	1.22E-06	1.02E-07	1.03E-09
		6	3.62E-07	3.01E-08	3.04E-10
	100	2	1.74E-05	1.93E-06	1.46E-08
		4	2.17E-06	2.41E-07	1.83E-09
		6	6.43E-07	7.14E-08	5.41E-10

2.4 Estimation of Available Power Generation

The useful (electric) power that can be generated solely from the enthalpy gain in all N laterals is a fraction of the thermal power produced and given by the expression

$$\dot{} \quad \text{Elec} \quad \dot{} \quad \text{)} - T_0 \big] \eta(\Gamma) \tag{23}$$

This useful power estimate does not include parasitic power due to frictional pressure drop in the vertical wellbores, and potential heat loss in the riser due to less than perfect insulation. Regardless of the EGS or AGS specifics, all of them use a pair of wells, and therefore the wellbore heat and pressure losses will be an additive constant. The thermal to electric conversion efficiency is the product of the Carnot and Thermal to Electrical conversion efficiencies according to

$$\eta(\Gamma) = \eta_{\text{Carnot}}(\Gamma)\,\eta_{\text{Conversion}}(\Gamma) \tag{24}$$

where the Carnot efficiency is

$$\eta_{\text{Carnot}}(\Gamma) = 1 - \frac{T_{\text{Exit}}(\Gamma) + 273.15}{T_{\text{in}} + 273.15} \tag{25}$$

and the Thermal to Electrical conversion efficiency is given by the cubic polynomial expression

$$\eta_{\text{Conversion}}(\Gamma) = \sum_{j=0}^{3} a_j \left[T_{\text{Exit}}(\Gamma) \right]^j \tag{26}$$

where it is assumed that there is minimal heat loss in the riser and that the turbine inlet temperature is practically the same as the riser (and hence the conduit) exit temperature. The physical exit temperature at the end of the laterals (entering the riser) is

$$T_{\text{Exit}}(\Gamma) = T_{\text{in}} + (T_{\text{Res}} - T_{\text{in}})(1 - e^{-\Gamma}) \tag{27}$$

and it is possible to define a dimensionless electric power as

$$\omega = \frac{\dot{W}_{\text{Elec}}}{N k_\infty L \Delta T} = \left[\frac{\dot{m} c_p}{k_\infty L}\right] \eta(\Gamma)(1 - e^{-\Gamma}) = \left[\left(\frac{\dot{m} c_p}{2\pi^n}\right) \frac{2\pi^n}{\bar{U} L}\left(\frac{\bar{U}}{k_\infty}\right)\right] \eta(\Gamma)(1 - e^{-\Gamma}) = 2\pi^n \text{Bi}\left[\frac{\eta(\Gamma)}{\Gamma}(1 - e^{-\Gamma})\right] \tag{28}$$

The algebraic manipulation in Eq. (28) above is to ensure that the mass flow rate which is the only available control parameter during the well operation is restricted to Γ, which is then effectively a proxy for the mass flow rate itself. Thus even though the Overall Heat Transfer Conductance term $\bar{U}$ is present in both Γ and the Biot Number, the optimum mass flow rate is a consequence of optimizing Γ such that the dimensionless electric power is maximised according to

$$\frac{\partial \omega}{\partial \Gamma} = 0 \tag{29}$$

so that the optimum value of Γ is independent of the Biot Number which declines with time as detailed in Appendix A. It is evident from Eq. (27) that this optimum value is a function of the inlet and resource temperatures. This relationship is depicted in Figure 3. The inflexion point is due to the cubic polynomial dependence of the thermal to electric power conversion efficiency. It is interesting to note that the optimum Γ falls within a fairly narrow range, across a wide range of resource temperatures.

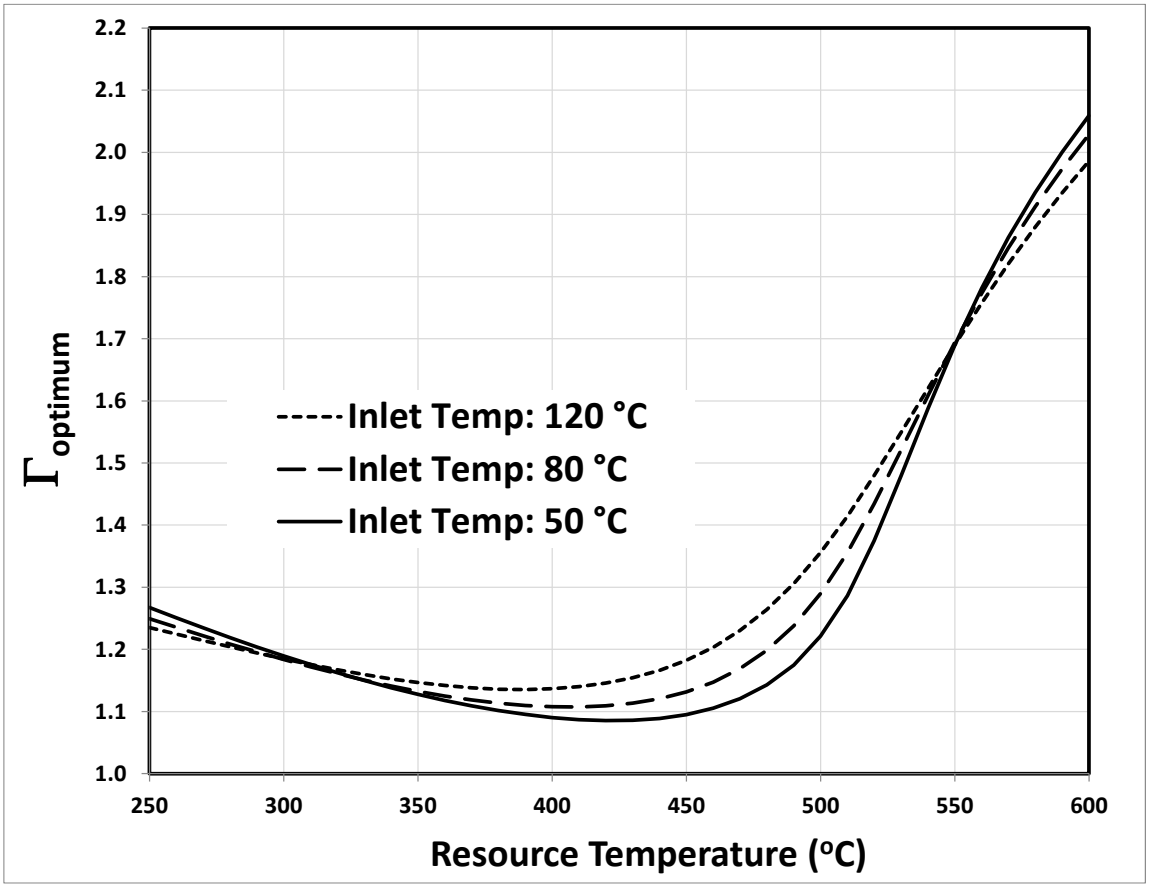

Figure 3: Optimum Γ as a function of resource and Inlet Temperatures

2.3 Thermal decline and Optimal Mass Flow Rate

With the passage of time, the cold front from the cold stream entering the laterals penetrates deeper into the formation effectively reducing the magnitude of the interface flux. This effect is captured in the Overall Conductance term (see Appendix A). The Modified Peclet Number as defined in Eq. (13) contains only the amass flow rate, so that given an optimum value of Γ obtained from Eq. (29), the segregation of the two is defined by

$$\left[\mathrm{Pe}_*\right]_{\mathrm{OPT}}(\tau)=\frac{\Gamma_{\mathrm{OPT}}}{\mathrm{Bi}(\tau)} \tag{30}$$

A compact representation of the Biot number encompassing both cylindrical and planar conduits is

$$\mathrm{Bi}=\frac{U(t)}{k_\infty}=\left(\frac{b}{w}\right)^{1-n}\left[\frac{2}{\mathrm{Nu}}\frac{k_\infty}{k}+\frac{1}{F_n(\tau_n)}\right]^{-1}\approx\left(\frac{b}{w}\right)^{1-n}F_n(\tau_n) \tag{31}$$

where the approximation follows from the fact that flow in the laterals is at a high Reynolds Number, and the convective flux magnitude is several orders of magnitude higher than the diffusive flux at the wellbore-formation interfaces. The consolidation of the Fourier Number definition accommodating both geometries is

$$\tau=\left[\frac{4n}{D^2}+\frac{1-n}{w^2}\right]\alpha_\infty t \tag{32}$$

The thermal decline as evidenced by the dependence of the optimum Modified Peclet Number (a proxy for mass flow rate) on the Fourier Number (a proxy for time) is shown in Figure 4 for 3 different values of the optimum Γ, for both cylindrical and planar geometries. For planar geometry, the decline at large times is seen to become independent of Γ_{OPT}, and therefore independent also of the inlet and resource temperatures.

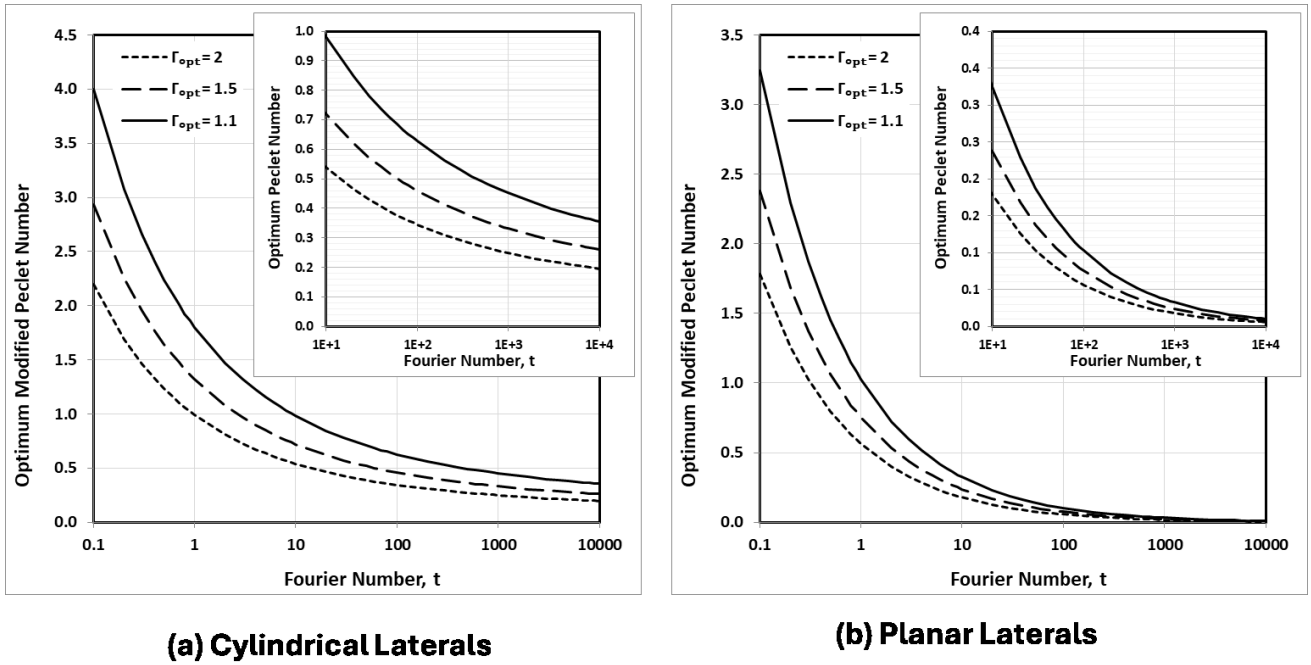

Figure 4: Peclet Number Decline with Fourier Number for Cylindrical (Left) and Planar (Right) Laterals

Substitution of Eq. (13) into Eq. (30) yields the optimum mass flow rate as a function of time as

$$\dot{m}=\left[\left(\frac{k}{c_p}\right)\mathrm{Bi}[\tau(t)]\right]\left[\frac{\Gamma_{\mathrm{OPT}}}{\Gamma_{\mathrm{OPT}}}\right] \tag{33}$$

where the constraint due to the wellbore's mass flow rate limitation is imposed. This limiting mass flow rate is a function of the injector and riser flow conduit size and is depicted for two riser sizes in Figure 5. It is assumed that insulation is possible even with a 8.5 in. riser with insulated coating, as is currently available for certain drill-pipes. The results in terms of both pressure differential and parasitic pump power are for each kilometer of Resource True Vertical Depth, and in both cases, a 8.5 in. Injector wellbore is assumed.

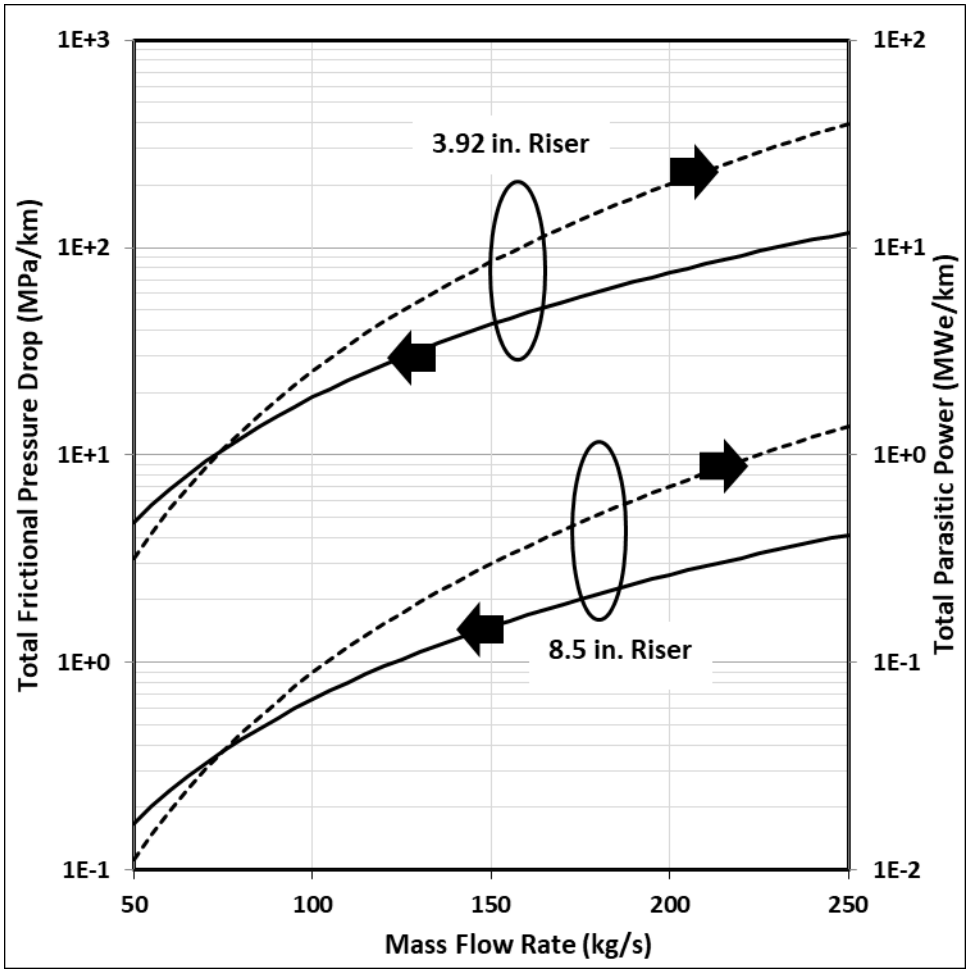

Figure 5: Wellbore Pressure Drop and Parasitic Power per kilometer of Resource Depth.

It should be noted that in calculating the net power, Γ must be re-evaluated from the resultant mass flow rate obtained from Eq. (33), as it may no longer correspond to the unconstrained optimum value based on that evaluated as a consequence of Eq. (29).

3., RESULTS AND DISCUSSION

The above analysis is best depicted using a couple of examples, which follow.

3.1 Case 1: 50 Fractured Planar Conduits over a 100 m Length

We first consider a scenario with a resource temperature of 400 ^{o}C at a depth of 5 km, and an inlet temperature of 100 ^{o}C. The injector and riser spaced 100 m apart are assumed to be connected by 50 planar conduits (fractures), each of width 3 mm, and a height of 50 m. The associated fluid and rock thermophysical properties are listed in Figure 6. In all of the panels in the figure, each vertical tick represents one year of elapsed time since the start of the flow.

The solid curve in the top panel shows the decay of the constrained optimal mass flow rate with time. As is obvious, the long-dashed line represents this wellbore-imposed limit.

A common operating technique has been to maintain the exit temperature (entering the riser) at the resource temperature. From Eq. (22), this would theoretically correspond to $\Gamma = \infty$ for the exit temperature to be exactly equal to the resource temperature, implying a mass flow rate tending to zero. To avoid this physically untenable scenario, we will assume that the exit temperature is actually 99% of the resource temperature. This corresponds then to a value of Γ given by

$$\Gamma_{\text{Max-T}} = -\ln \varepsilon \tag{34}$$

where $\varepsilon = 0.01$. The mass flow rate associated with $\Gamma_{\text{Max-T}}$ is accordingly given by

$$\dot{m} = \frac{\Gamma(t) L}{1_{\text{Max-T}} c_p} \tag{35}$$

and indicated by the short-dashed curve in the top panel of Figure 6.

The middle panel of Figure 6 shows the decline of the gross available electric power which as a reminder, does not account for parasitic losses in the wellbore (an additive constant). If the goal is the maximum power generation possible, the optimized power generation schedule outperforms that corresponding to the maximum arrival temperature schedule by a factor of 2 over a 10 year operating horizon, and with a power generation capacity over 1 MWe. By contrast, the maximum arrival temperature schedule falls below this 1 MWe threshold at the end of 5 years. What is noteworthy is that maintaining the mass flow rate at the wellbore limit results in a significant reduction in power generation, thereby highlighting the importance of the optimum mass flow rate schedule.

The lowermost panel of Figure 6 shows the exit temperature for each of the three operating scenarios. Once the wellbore-imposed mas flow rate constraint is no longer active, the exit temperature remains constant as is consistent with the optimum value of Γ that as the reader will recall is solely a function of inlet and resource temperatures as evidenced in Figure 3. An important consideration in the use of the optimized mass flow rate, as opposed to holding it at the wellbore limit is that in the former is associated with a substantially higher exit temperature. This could have implications with respect to the surface power generation equipment, particularly with regard to the heat exchanger component of the ORC in the event one is used.

3.2 Case 2: 50 Fractured Planar Conduits over a 250 m Length

If the same 50 connecting fractures as in Case 1 were extended to 250 m, the middle panel of Figure 7 shows that the optimized mass flow rate schedule results in 3 Mwe at the end of the 10 year horizon – a threefold increase over that corresponding to a 100 m length. It is seen from the inset in the uppermost panel that during approximately the first two months (8 weeks) the optimum is constrained by the maximum permissible mass flow rate allowed by the wellbores. There is still a substantial benefit from using the optimized mass flow rate as opposed to that corresponding to the maximum arrival temperature. If the flow is kept at the wellbore maximum permissible it is seen from the lowermost panel of Figure 7 that the exit temperature is probably too low to sustain any reasonable power production.

3.3 Case 3: 100 Fractured Planar Conduits over a 250 m Length

Even better performance is obtained if a 100 connecting fractures are achieved over the 250 m length as shown in Figure 8. While this may be at the outer edge of feasibility with current operational practices, the benefit of being able to produce a minimum of 6 Mwe over a 10 year horizon is a payoff that is perhaps worth the effort. This is twice the power of sub-optimal mass flow rate schedules as seen in the middle panel of the figure. In this case, the wellbore constraint on the optimal mass flow rate extends out toa little over the first 7 months (32 weeks) of operation as seen in the top panel.

3.2 Case 4: 50 Drilled Cylindrical Laterals

We next consider a case with each of the 3 mm thick by 50 m high fractures replaced by a cylindrical drilled later of diameter 3 in. The trends in Figure 9 corresponding to this case are very similar to those observed in the preceding case with planar geometry As will be noted in the top panel, the optimum mass flow rates are substantially lower with cylindrical laterals. This is on account of the much lower contact area to surface area ratio associated with cylindrical laterals. In face comparing the geometrical data of the fractures in the two cases, it is seen that there is a sixfold increase in the A_c / A_f ratio associated with the planar conduits.

The lower mass flow rates accordingly result in a substantial decrease in the power generation capacity with a sub-megawatt threshold being reached very shortly after the start of the flow period. While this study does not consider the monetary aspects of the operation, it is hard to envisage a scenario in which this case would be economically feasible.

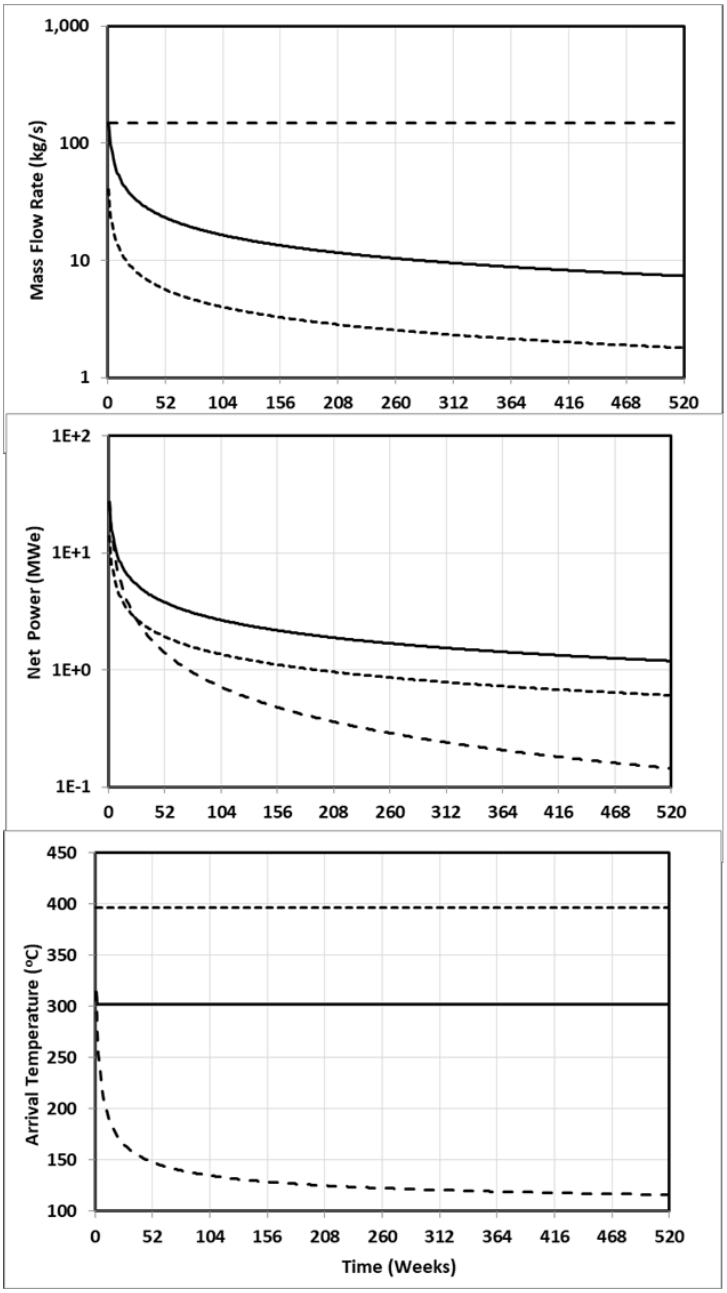

Maximum Power

Wellbore Mass Flow Rate Limit

Maximum Arrival Temperature

Inlet Temperature (°C)	100
Resource Temperature (°C)	400
Formation Thermal Conductivity (W/m-K)	2.0
Formation Thermal Diffusivity (m^2/s)	8.00E-07
Water Specific Heat (J/kg-K)	4,316
Number of Conduits	50
Lateral Length (m)	100
Resource Depth (m)	5000
Fracture Width (mm)	3.00
Fracture Height (m)	50

Figure 6: Constrained Optimal Mass Flow Rate Schedule (Top), Net Power (Middle) and Exit Temperature (Bottom) with 50 Planar Conduits of Length 100 m across a Resource at Temperature 400 °C.

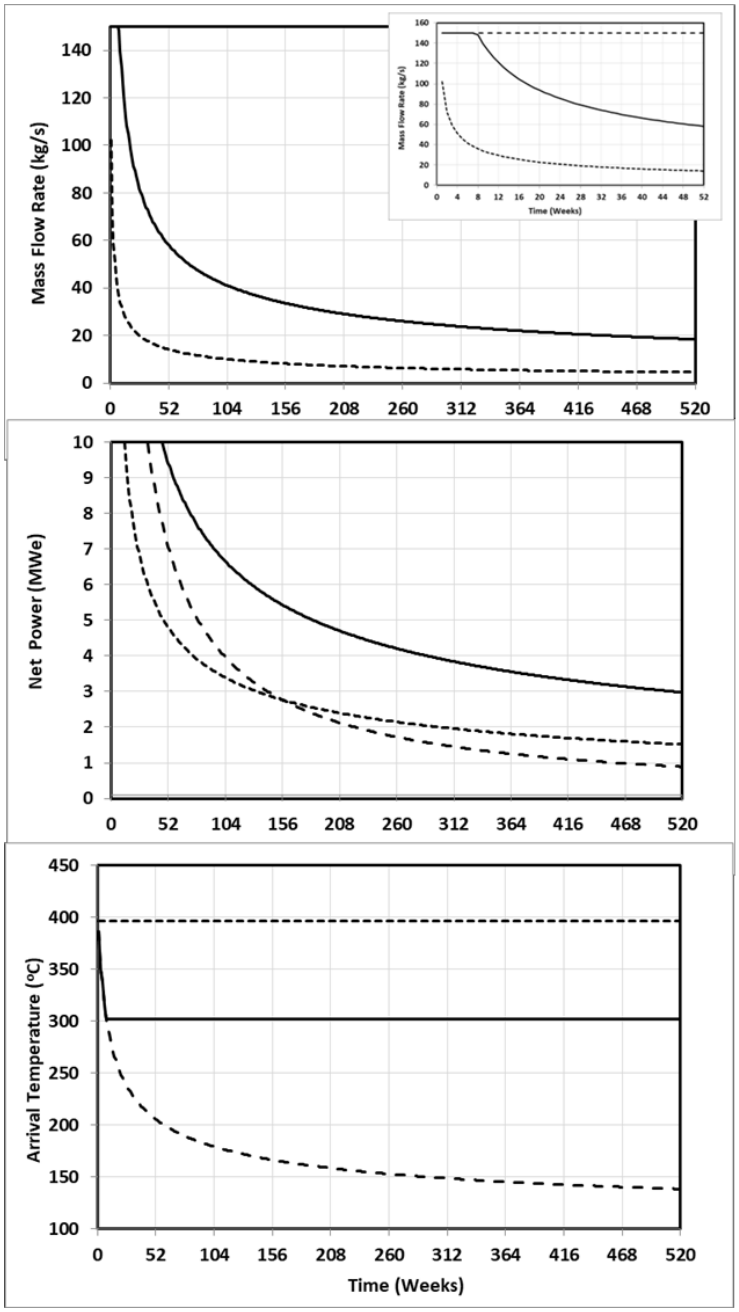

Inlet Temperature (°C)	100
Resource Temperature (°C)	400
Formation Thermal Conductivity (W/m-K)	2.0
Formation Thermal Diffusivity (m^2/s)	8.00E-07
Water Specific Heat (J/kg-K)	4,316
Number of Conduits	50
Lateral Length (m)	250
Resource Depth (m)	5000
Fracture Width (mm)	3.00
Fracture Height (m)	50

Figure 7: Constrained Optimal Mass Flow Rate Schedule (Top), Net Power (Middle) and Exit Temperature (Bottom) with 50 Planar Conduits of Length 250 m across a Resource at Temperature 400 °C.

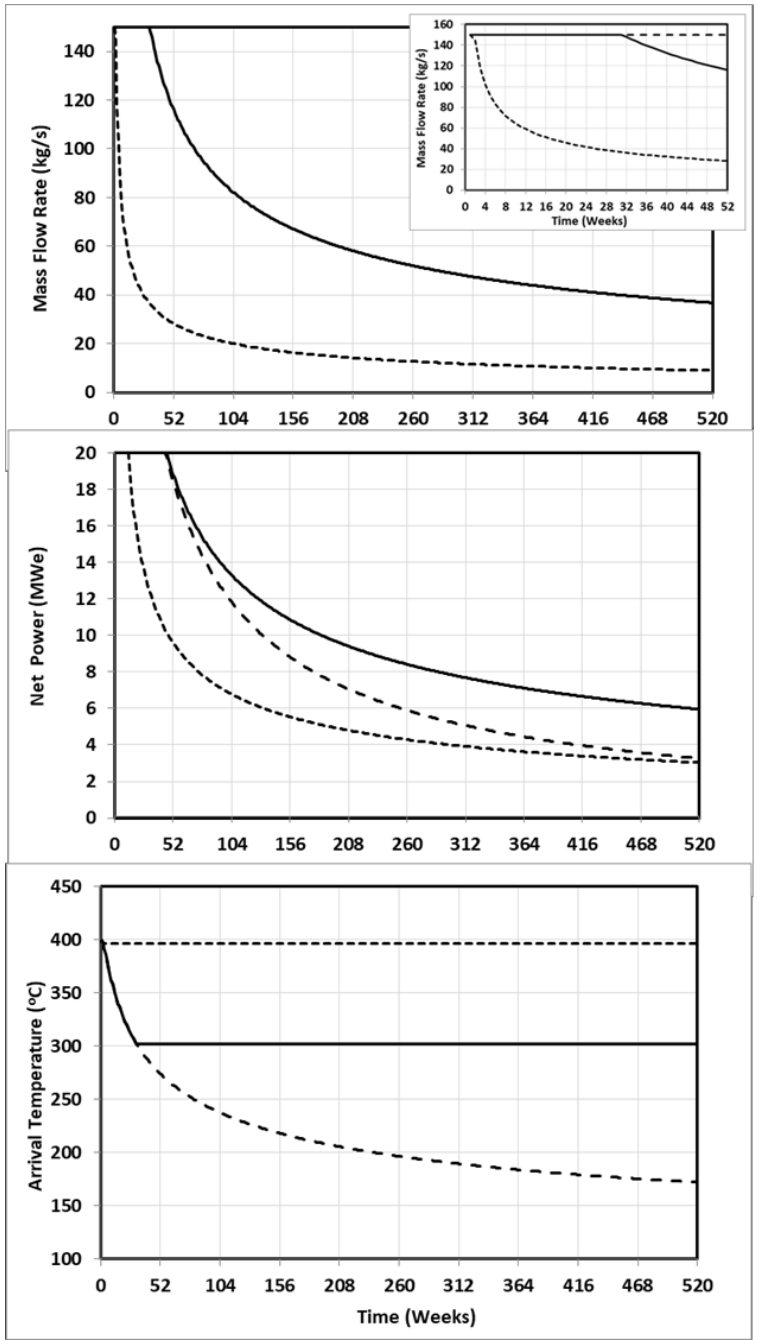

Maximum Power

Wellbore Mass Flow Rate Limit

Maximum Arrival Temperature

Inlet Temperature (°C)	100
Resource Temperature (°C)	400
Formation Thermal Conductivity (W/m-K)	2.0
Formation Thermal Diffusivity (m^2/s)	8.00E-07
Water Specific Heat (J/kg-K)	4,316
Number of Conduits	100
Lateral Length (m)	250
Resource Depth (m)	5000
Fracture Width (mm)	3.00
Fracture Height (m)	50

Figure 8: Constrained Optimal Mass Flow Rate Schedule (Top), Net Power (Middle) and Exit Temperature (Bottom) with 100 Planar Conduits of Length 250 m across a Resource at Temperature 400 °C.

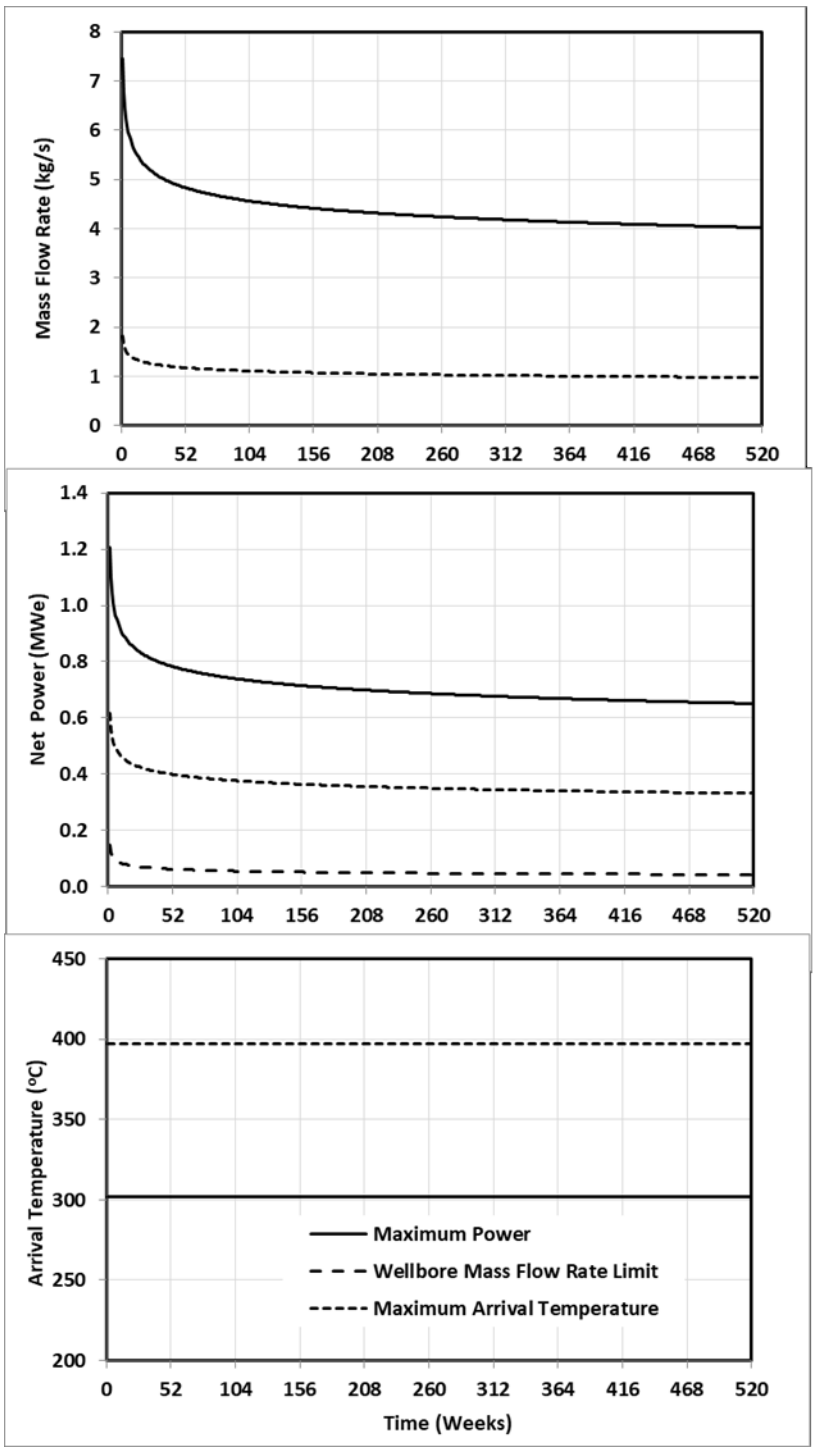

Inlet Temperature (°C)	100
Resource Temperature (°C)	400
Formation Thermal Conductivity (W/m-K)	2.0
Formation Thermal Diffusivity (m^2/s)	8.00E-07
Water Specific Heat (J/kg-K)	4,316
Number of Laterals	10
Lateral Length (m)	1000
Resource Depth (m)	5000
Diameter (in)	3.00

Figure 9: Constrained Optimal Mass Flow Rate Schedule (Top), Net Power (Middle) and Exit Temperature (Bottom) with 10 Cylindrical Laterals of Length 1 km across a Resource at Temperature 400 °C.

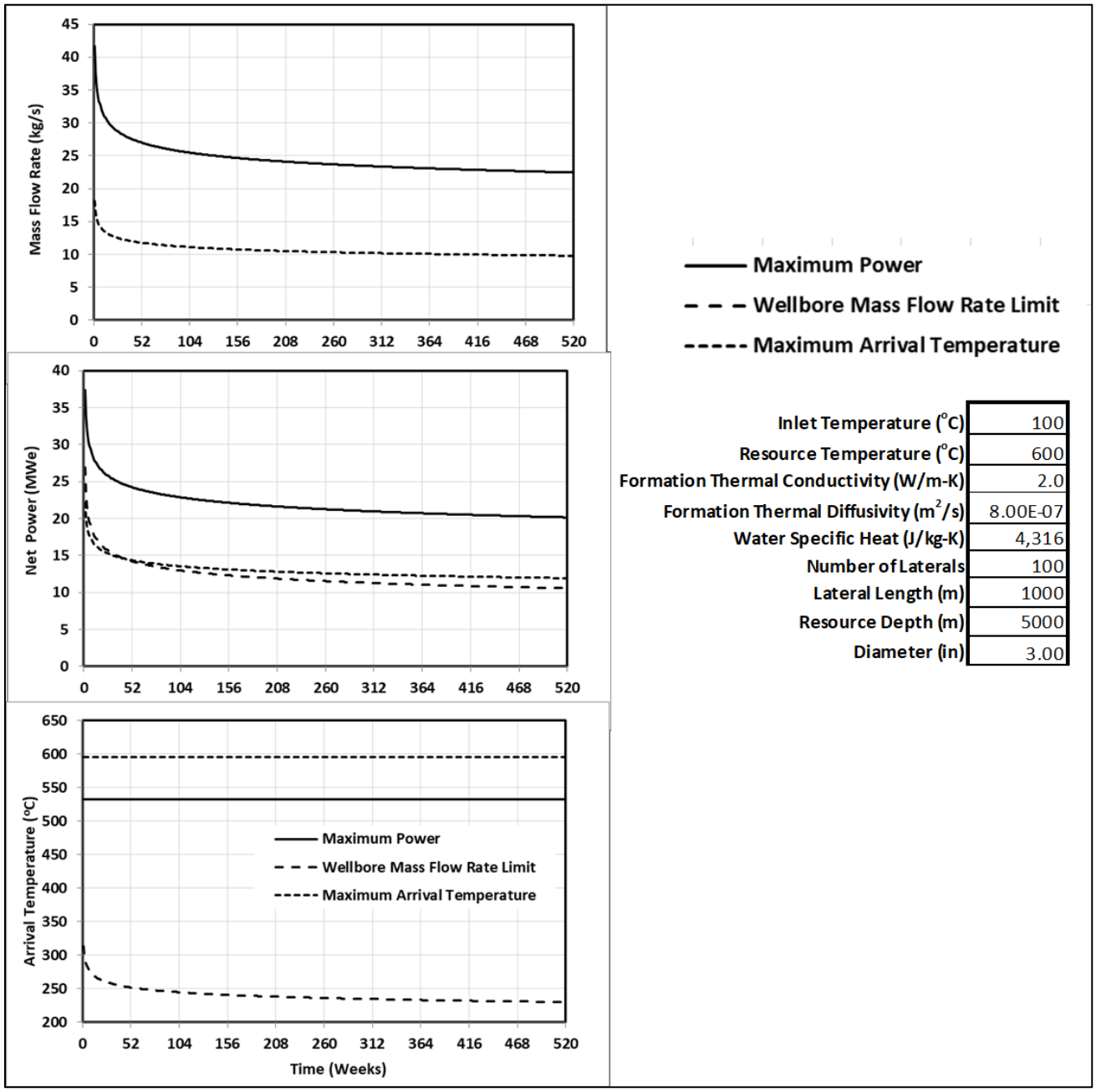

Figure 10: Constrained Optimal Mass Flow Rate Schedule (Top), Net Power (Middle) and Exit Temperature (Bottom) with 10 Cylindrical Laterals of Length 1 km across a Resource at Temperature 400 °C.

4. CONCLUSIONS

This works extends the previous work by Chandrasekhar et al. (2024) to consider optimization of electric power in any EGS or AGS system. The non-dimensional governing equations are solved semi-analytically. We define a nondimensional parameter Γ that governs the performance of any EGS or AGS system. Γ is a function of three important dimensionless groupings: the ratio of the Biot and Peclet number, the ratio of the resource conductivity to working fluid conductivity, and the ratio of the conduit contact area to the flow area. The previous solution is extended to express Γ in terms of a modified Peclet number, which is a proxy for mass flow rate. An expression for nondimensional power is then developed in terms of Γ. The decline in performance is also considered, by relating Γ to the Fourier number. Two examples (fracture connectivity and drilled lateral connectivity) are shown to illustrate the method. It is shown that maximizing arrival temperature does not maximize power generated. Indeed, by managing operations such that Γ is at or near its optimum value as a function of time, the power performance of an EGS or AGS system can be maximized. With the larger number of connecting conduits,

fractures are seen to outperform cylindrical drilled laterals even over much shorter lengths. While conceptually obvious, the benefits of larger fracture lengths and number of fractures are quantified.

REFERENCES

Chandrasekhar, S., Suryanarayana, P.V., Sathuvalli, U.B., and Asher, G.: Scaling and Thermal Penetration Depth in Enhanced Geothermal Energy Production, GRC Transactions Vol. 48, Waikiloa, HI (2024).

R. Allis, and J. N. Moore, 2019, Geothermal Characteristics of the Roosevelt Hot Springs System and Adjacent FORGE EGS Site, Milford, Utah, Utah Geological Survey.

Beckers, K.F., Rangel-Jurado, N., Chandrasekar, H., Hawkins, A.J., Fulton, P.M., and Tester, J.W., 2022, "Techno-Economic Performance of Closed-Loop Geothermal Systems for Heat Production and Electricity Generation", Geothermics, v. 100, p. 102318.

Brown, D., Duchane, D., Heiken, G., and Hriscu, V., 2012, Mining the Earth's Heat: Hot Dry Rock Geothermal Energy, Springer

Carslaw, H. S., and Jaeger, J. C., Conduction of Heat in Solids, Oxford Clarendon Press, 1959.

Chandrasekhar S. Revisiting the Classical Problem of Transient Temperature Prediction in Complex Deepwater Wellbores with a New Semi-Analytical Approach", SPE/IADC Paper 199653. Galveston, TX , March 3--5, 2020.

Gringarten, A. C., Witherspoon, P. A., and Ohnishi, Y., 1975, "Theory of Heat Extraction from Fractured Hot Dry Rock", Journal of Geophysical Research, Vol 80, N0. 8, 1975.

Holmes, M., Toews, M, Jenkins, J., and Sepulveda, N., 2021, Multilateral Closed-Loop Geothermal Systems as a Zero Emission Load-Following Resource, GRC Transactions, Vol. 45.

Moncarz, P. D., and Suryanarayana, P. V., 2022, "Harvesting GeoHeat and the Impact of Enhancing Thermal Reach on Energy from Hot Dry Rock", United States Military Academy Special Colloquium on Computational Engineering Mathematics, West Point, October 21-22

Norbeck, J., Latimer, T., Gradl, C., Agarwal, S., Dadi, S., Eddy, E., Fercho, S., Lang, C., McConville, E., Titov, A., Voller, K., and Woitt, M., 2023, "A Review of Drilling and Stimulation of a Horizontal Geothermal Well System in North Central Nevada", 48th Stanford Geothermal Workshop, February 6-8, 2023.

M. N. Özisik, 1993, Heat Conduction, 2nd Edition, J. Wiley & Sons.

H. J. Ramey, Jr., 1962, "Wellbore Heat Transmission", SPE Paper 96, March 1962.

Suryanarayana, P. V., Chandrasekhar, S. V., and Asher, G., 2023, "A Review of Recent Concepts for Geothermal Energy Extraction with Focus on Thermal Reach", 3rd Philippine International Geothermal Conference, Manila, The Philippines.

US Department of Energy, "Pathways to Commercial Liftoff: Next-Generation Geothermal Power", Public Report, March 2024.

NOMENCLATURE

A_c	m^2	Contact Area
A_f	m^2	Flow Area
b	m	Fracture Width
Bi		Biot Number
c_{JT}	m^2/N	Joule Thomson Coefficient
c_p	J/kg-K	Fluid Specific Heat
d	m	Conduit Diameter
D_h	m	Hydraulic Diameter
f		Friction factor
h	W/m^2-K	Heat Transfer Coefficient
k	W/m-K	Thermal Conductivity
L	m	Conduit Length
$\dot{m}$	kg/s	Mass Flow Rate
n		Geometry Index (0 or 1)
P	N/m^2	Fluid Pressure
Pe		Peclet Number
$\dot{q}$	W/m	Heat Flux per Unit Length

t	s	Operation Time
T	°C	Working Fluid Temperature
V	m/s	Bulk Velocity
w	m	Fracture Thickness
U	W/m-K	Overall Heat Transfer Conductance
x	m	Lateral Distance into Formation from fracture Surface
z	m	Streamwise Distance

Greek Symbols

α	m^2	Thermal Diffusivity
Γ	kg/s	Number of Transfer Units
η		Efficiency (Carnot or Conversion)
Λ	s	Dimensionless Frictional Heating Parameter
θ		Dimensionless Fluid Temperature
ρ	kg/m^3	Density
τ		Fourier Number (Dimensionless time)
ω		Dimensionless Electric Power
ξ		Dimensionless Streamwise Coordinate

Subscripts

A_f	Flow Area
$\dot{m}$	Mass Flow Rate
Exit	Conduit Exit Condition
f	Fluid
in	Conduit Inlet Condition
OPT	Optimal Value
W	Conduit/Formation Interface
∞	Surrounding Hot Rock

APPENDIX A: OVERALL HEAT TRANSFER CONDUCTANCE

A.1 Cylindrical Conduits

Equating the convective flux at the inner surface of the conduit-formation interface to the diffusive flux on the outside surface yields the expression

$$\dot{Q} = \frac{D}{2}\left(T_W - T\right) = 2\pi k_\infty \frac{D}{2}\frac{\partial T}{\partial x}(t)\bigg|_{x=\frac{w}{2}} = 2\bar{U}\left(T_\infty - T\right) \tag{36}$$

in which the factor of 2 accounts for the two surfaces of the conduit in contact with the formation. The last equality enables the flux to be expressed in terms of the difference between the fluid and undisturbed geothermal temperature difference. The diffusive flux can be expressed as

$$k_\infty \frac{d}{2}\frac{\partial T}{\partial x}\bigg|_{r=\frac{D}{2}} = k_\infty\left(T_\infty - T_W\right)F(\tau) \tag{37}$$

where the thermal decline is a function of the Fourier Number τ according to

$$F(\tau) = \frac{\partial\theta}{\partial\eta}(\tau)\bigg|_{\eta=1} = \mathrm{L}^{-1}\left[\frac{1}{\sqrt{s}}\frac{K_1\left(\sqrt{s}\right)}{K_o\left(\sqrt{s}\right)}\right]\begin{cases} = \dfrac{1}{\sqrt{\pi\tau}}, & \tau \le 0.001, \\ \approx 10^{\sum_{k=0}^{5} p_k (\log_{10}\tau)^k}, & \tau > 0.001 \end{cases} \tag{38}$$

The reader is referred to Van Everdingen and Hurst (1942) for the derivation of Eq. (38). The flux continuity exemplified in Eq. (36) results in

$$\frac{\bar{U}}{k_\infty}=\left[\frac{2k}{hD}\frac{k_\infty}{k}+\frac{1}{F(\tau)}\right]^{-1}=\left[\frac{k_\infty}{k}\frac{2}{\mathrm{Nu}}+\frac{1}{F(\tau)}\right]^{-1} \tag{39}$$

The Fourier Number in the case of a rectangular conduit is defined as

$$\tau=4\frac{\alpha_\infty}{D^2}t \tag{40}$$

A.2 Planar Conduits

Equating the convective flux at the inner surface of the conduit-formation interface to the diffusive flux on the outside surface yields the expression

$$\dot{Q}\quad\text{---}\,\text{W}-T\right)=2k_\infty b\frac{\partial T}{\partial x}(t)\Big|_{x=\frac{w}{2}}=2\bar{U}\left(T_\infty-T\right) \tag{41}$$

in which the factor of 2 accounts for the two surfaces of the conduit in contact with the formation. The last equality enables the flux to be expressed in terms of the difference between the fluid and undisturbed geothermal temperature difference. The diffusive flux can be expressed as

$$k_\infty b\frac{\partial T}{\partial x}\Big|_{x=\frac{w}{2}}=k_\infty\frac{b}{w}\left(T_\infty-T_\mathrm{W}\right)F\left(\tau\right) \tag{42}$$

where the thermal decline is a function of the Fourier Number τ according to

$$F\left(\tau\right)=\frac{\partial\theta}{\partial\eta}(\tau)\Big|_{\eta=1}=\frac{1}{\sqrt{\pi\tau}} \tag{43}$$

The derivation of Eq. (43) is shown in the graphic of Figure 11. A modicum of algebra leads to

$$\frac{\bar{U}}{k_\infty}=\frac{b}{w}\left[\frac{k}{hw}\frac{k_\infty}{k}+\frac{1}{F\left(\tau\right)}\right]^{-1}=\frac{b}{w}\left[\frac{2}{\mathrm{Nu}}\frac{k_\infty}{k}+\frac{1}{F\left(\tau\right)}\right]^{-1} \tag{44}$$

The Fourier Number in the case of a rectangular conduit is defined as

$$\tau=\frac{\alpha_\infty}{w^2}t \tag{45}$$

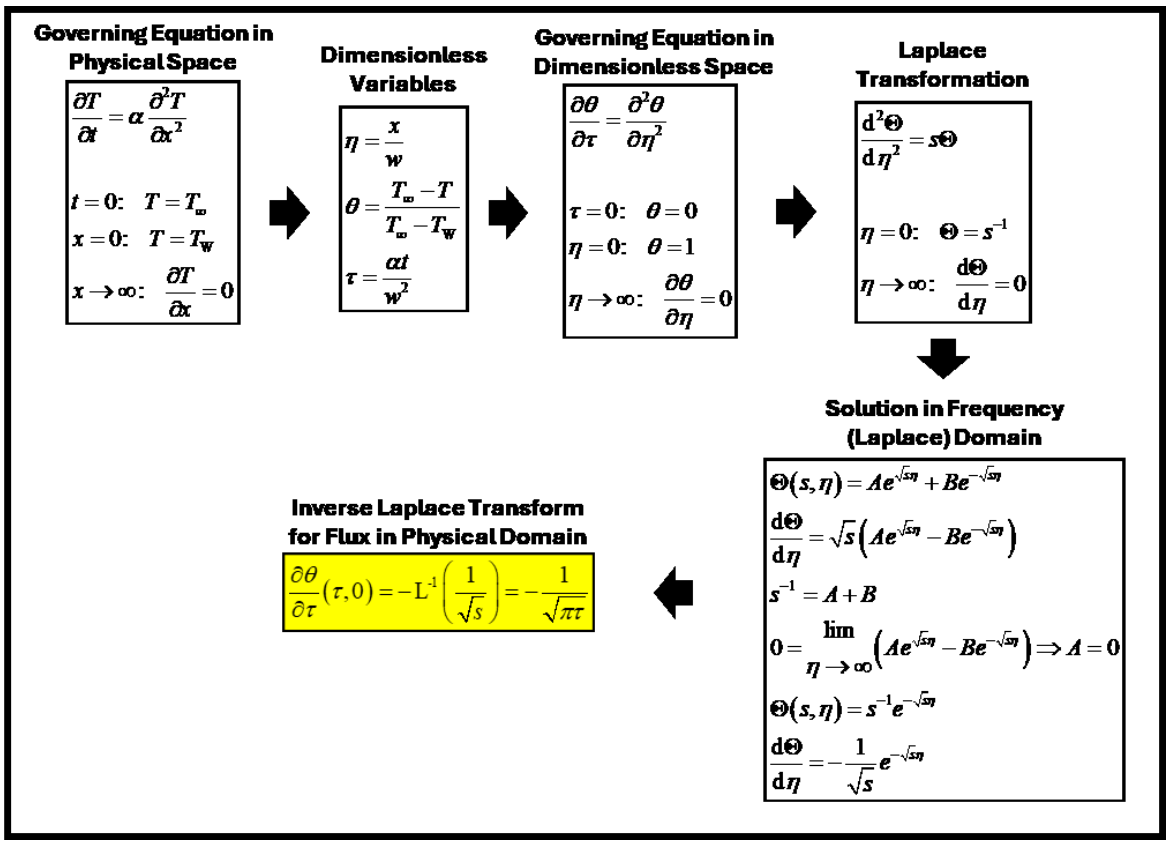

Figure 11: Derivation of the Transient Interface Heat Flux in a Planar Conduit.